Pediatric Radiology
https://doi.org/10.1007/s00247-021-05090-z

PEDIATRIC BODY MRI

Practical protocol for lung magnetic resonance imaging and common clinical indications

Kushaljit Singh Sodhi[1] · Pierluigi Ciet[2,3] · Shreyas Vasanawala[4] · Juergen Biederer[5,6,7,8]

Received: 30 November 2020 / Revised: 23 February 2021 / Accepted: 20 April 2021

Abstract
Imaging speed, spatial resolution and availability have made CT the favored cross-sectional imaging modality for evaluating various respiratory diseases of children — but only for the price of a radiation exposure. MRI is increasingly being appreciated as an alternative to CT, not only for offering three-dimensional (3-D) imaging without radiation exposure at only slightly inferior spatial resolution, but also for its superior soft-tissue contrast and exclusive morpho-functional imaging capacities beyond the scope of CT. Continuing technical improvements and experience with this so far under-utilized modality contribute to a growing acceptance of MRI for an increasing number of indications, in particular for pediatric patients. This review article provides the reader with practical easy-to-use protocols for common clinical indications in children. This is intended to encourage pediatric radiologists to appreciate the new horizons for applications of this rapidly evolving technique in the field of pediatric respiratory diseases.

Keywords Chest · Children · Lungs · Magnetic resonance imaging · Pulmonary

Introduction

Imaging plays a significant role in the assessment of various lung diseases in the pediatric population. It is used in the initial detection and characterization of various congenital and acquired lung disorders in children that are often difficult to diagnose clinically. Traditionally, a chest radiograph is the most common and often the first radiologic investigation performed worldwide in children. It is adequate in many clinical conditions involving the pulmonary system. However, often it is nonspecific and non-contributory. Lung US can also serve as the initial examination, but its diagnostic scope, in particular for central parts of the lung, is limited. Therefore, additional cross-sectional imaging is required for many specific clinical applications. CT provides additional anatomical and pathological information but involves radiation exposure, which can have detrimental effects in children. Although improvements in CT detector technology have increased the efficiency of the imaging systems, radiation exposure remains a matter of concern. Given the high sensitivity of children to radiation

✉ Kushaljit Singh Sodhi
sodhiks@gmail.com

[1] Department of Radiodiagnosis,
Post Graduate Institute of Medical Education & Research (PGIMER),
Sector-12, Chandigarh 160012, India

[2] Department of Paediatric Pulmonology and Allergology,
Erasmus MC – Sophia Children's Hospital,
Rotterdam, The Netherlands

[3] Department of Radiology and Nuclear Medicine,
Erasmus MC,
Rotterdam, The Netherlands

[4] Department of Radiology,
Stanford University,
Stanford, CA, USA

[5] Department of Diagnostic and Interventional Radiology,
University Hospital of Heidelberg,
Heidelberg, Germany

[6] Translational Lung Research Center Heidelberg (TLRC),
German Lung Research Center (DZL), Heidelberg, Germany

[7] Faculty of Medicine,
University of Latvia,
Riga, Latvia

[8] Faculty of Medicine,
Christian-Albrechts-Universität zu Kiel,
Kiel, Germany

Published online: 26 May 2021

exposure and their long-time horizon to manifest any radiation-related risks of malignancy, any alternative is highly appreciated [1].

Earlier, MRI applications in the lungs were quite limited because of the low proton density (weak signal), the cardiac and respiratory motion, and susceptibility artifacts. Advances in lung MR imaging technology in the last decade have changed the way we image the lungs, offering adequate and comparative radiologic information relative to CT in some specific clinical indications. It has the advantage of being non-ionizing and can thus be repeated in children without any radiation risks. Lung MRI also offers functional evaluation and provides ventilation and perfusion assessment at the same sitting [2, 3]. In this review, we present common practical MRI protocols that can be employed in routine clinical practice along with common clinical indications in which lung MRI can be used optimally.

Patient preparation

Children up to 5 years frequently cannot follow breath-hold instructions, and therefore free-breathing MRI techniques with sedation or anesthesia are mandatory. In neonates and children up to 6 months, the feed-and-swaddle technique can be used efficiently. Children who can follow breathing instructions can undergo MRI without sedation with adequate preparation and training. Training is needed to familiarize the child with the MRI environment and specific breathing maneuvers can be practiced prior to MRI. A respiration belt or cushion for respiratory motion feedback and triggering or gating during the examination is considered helpful. Lung volume standardization can also be enhanced using an MRI-compatible spirometer [4–6]. To further reduce anxiety, parents can be allowed to stay inside the MRI room with the child.

Magnetic resonance imaging system and pulse sequence selection

System and coil selection

Generally, standard 1.5-tesla (T) systems provide a more favorable platform than higher field strengths to perform lung MRI, given the lower susceptibility-related signal loss when using conventional sequences. However, 3-T equipment frequently offers higher gradient performance. In particular, because three-dimensional (3-D) gradient echo imaging of the lung yields better results at higher field strengths, the use of high field systems is explicitly not discouraged [7, 8]. Appropriate coil receiver selection also influences image quality, where multi-channels coils, namely torso coils with 16 or 32 channels, are the most frequently used. Close-fitting coils provide higher signal-to-noise ratio (SNR) because of their closer proximity to the lungs. Therefore, coil selection should be tailored to the clinical question of the MRI study. For instance, for exams of the central airways in young children (<6 years), a smaller, flexible and lightweight coil array in direct contact with the anterior chest wall is preferred. Conversely, older children (≥6 years) can be imaged with a torso or head/neck/spine coil array.

Pulse sequence selection

Similar to CT, lung MRI can be performed with breath-hold or free-breathing acquisitions. Breath-hold (inspiratory and expiratory) acquisitions can only be achieved in children who can follow breathing instructions. Breath-hold time should be tailored to the child's abilities, which can be estimated in a short training session before the MRI examination. Children–of age group 6–12 years often require shorter acquisition time (6–10 s). Children younger than 6 years should be preferably examined using gated free-breathing acquisitions with respiratory triggering or navigator-based techniques at the expense of longer measurement times. To balance scan time, free-breathing acquisitions, such as PROPELLER (periodically rotated overlapping parallel lines with enhanced reconstruction), ultra-short echo-time (UTE) imaging and zero echo-time (ZTE) imaging should be implemented with an acquisition time per sequence of 5–10 min to allow for acquisitions with different weighting. Total scan time is usually no longer than 30 min.

Several two-dimensional (2-D) or 3-D techniques can be used for lung MRI. A basic lung MRI protocol is presented in Table 1 [9]. Select sequences can be performed in individual cases, depending on the clinical details, and all the given sequences are not required in all cases. These can—be further standardized at individual institutions and optimized.

Two-dimensional techniques

Two-dimensional techniques have unequal voxel dimensions (anisotropic) and cannot be used for reformats in other viewing planes. Two-dimensional techniques include spin-echo and gradient echo sequences. Spin-echo sequences are a robust technique with limited signal loss from field inhomogeneities. Spin-echo sequences are usually acquired with T2 weighting, with or without fat-saturation techniques, and they provide higher contrast for fluid detection. Different acronyms are used, depending on the MRI scanner manufacturer. T2-W sequences enable assessment of bronchial wall thickening and mucus plugging. Bronchial wall imaging can be further improved with black-blood preparations [10, 11] using heavy T2 weighting (longer effective echo time). Black-blood preparation removes signal of pulmonary vessels, facilitating detection of bronchiectasis, mucus plugging and small nodules.

Table 1 Pulse sequence selection for lung MRI in children

Contrast	Sequence type[a]	Protocol suggestion[b]				<6 years[c]		6–12 years[c]		>12 years[c]	
		Basic protocol	Airway disease	Vessel disorders	Malig-nancy	Acquisition mode[d]	Acquisition time[e]	Acquisition mode[d]	Acquisition time[e]	Acquisition mode[d]	Acquisition time[e]
T1	• 2-D gradient echo (2-D GRE)	Tran 1/2 options[f]				Free-breathing triggered or navigated	2–3 min	Breath-hold	<10 s	Breath-hold	<20 s
	• 3-D gradient echo (3-D GRE)		Tran + cor		Tran						
T2	• Fast spin echo (FSE) • FSE with fat suppression • Spin-echo inversion recovery (IR)	Tran + cor 1/4 or 2/4 options[f]	Tran or cor	Tran or cor	Tran + cor 1/2 or 2/2 options[f]	Triggered	5–10 min	Triggered or multi-breath-hold	5–10 min or 3–5 min	Multi-breath hold	3–5 min
	• FSE half-Fourier		Tran or cor	Tran or cor		Free-breathing	<20 s	Breath-hold	<10 s	Breath-hold	<20 s
T1/T2	Steady-state free precession (SSFP)	Tran or cor (Sag)		Tran + cor (Sag)	Tran or cor (Sag)	Free-breathing	<1 min	Breath-hold or free-breathing	<10 s or <1 min	Breath-hold or free-breathing	<20 s or <1 min
PD	3-D GRE ultrashort echo time	(Cor)	Cor		Tran	Free-breathing navigated	5–10 min	Free-breathing navigated	5–10 min	Free-breathing navigated	5–10 min
DWI	DWI fast imaging (e.g., EPI)									Multi-breath-hold	3–5 min
T1 DCE (IV CM)	Time-resolved keyhole GRE		(Cor)	Cor		Free-breathing	<1 min	Free-breathing	<1 min	Breath-hold + free-breathing	<1 min
T1 MRA (IV CM)	3-D GRE		(Cor)	Cor		Free-breathing	<10 s	Breath-hold	<10 s	Breath-hold	<20 s
T1 (IV CM)	• 3-D GRE with fat suppression			Tran + cor 1/2 options[f]	Tran + cor 1/2 options[f]	Free-breathing navigated	2–3 min				
	• 3-D GRE Dixon					Free-breathing navigated	2–3 min				

2-D two-dimensional, *3-D* three-dimensional, *CM* contrast media, *cor* coronal slice orientation, *DCE* dynamic contrast-enhanced, *DWI* diffusion-weighted imaging, *EPI* echoplanar imaging, *IV* intravenous, *min* minutes, *MRA* magnetic resonance angiography, *PD* proton-density, *s* seconds, *sag* sagittal orientation, *tran* transverse slice orientation

[a] Generic sequence names; for translations into vendor-specific sequence names see Biederer et al. [9]

[b] Parentheses indicate additional, optional orientations

[c] Depending on the ability of the child to cooperate

[d] Options for triggering, gating, navigating or self-navigating might differ among vendors and need to be selected according to availability

[e] Acquisition times are only a rough estimation and might differ significantly, in particular for triggered or gated/navigated sequences

[f] 1/2, 1/4, 2/2 refers to the choice of selection of sequence types, suggesting use of, e.g., 1 of the 2 available sequence types, 1 of the 4, etc.

Gradient echo steady-state free precession (SSFP) sequences provide mixed-weighting T2/T1, which enhances the visibility of lung tissues with water-like characteristics, such as mucus plugs in the airways. Two-dimensional SSFP sequences can cover the entire thorax in a single breath-hold with a good image quality. Two-dimensional SSFP sequences are also used for non-contrast angiographic imaging because vascular structures appear consistently bright, thereby allowing assessment of mediastinal vessels.

Routinely, electrocardiogram (ECG) gating is not used to avoid too long an acquisition time. However, ECG triggering is important to eliminate artifacts around the heart, and this might be important to assess pathology in middle lobe and lingula regions.

Three-dimensional techniques

Three-dimensional techniques enable isotropic voxel collection, which enables reformats to arbitrary viewing planes. Three-dimensional techniques are particularly important to review central airway pathology. Typically, 3-D techniques are based on gradient echo sequences with short and ultrashort echo times (TE). Gradient echo sequences are considered the most robust acquisition format for lung MRI. Full chest coverage with isotropic voxel sizes between 2.0 mm and 3.5 mm can be achieved in a single breath-hold of less than 10 s. Gradient echo sequences enable both proton-density (using a low flip angle) and T1 weighting (T1-W at higher flip angles). Proton-density weighted acquisitions are frequently used to assess airways without the use of contrast agents and air-trapping in end-expiratory images. T1-W is used to assess pulmonary vasculature and lung parenchymal perfusion when combined with contrast administration [9–11].

Functional imaging

One of the main advantages of MRI over CT is its ability to provide information about several functional aspects of lung and airways. When combined with contrast injections, both the pulmonary vasculature and lung perfusion can be studied effectively. Dynamic MR imaging (cine MRI) can be used to assess either central airways or diaphragm mechanics. Using hyperpolarized gases, such as helium (^{3}He) and xenon (^{129}Xe), high-contrast images of lung ventilation can be obtained. By using a new experimental technique known as Fourier decomposition, lung ventilation and perfusion maps without gaseous and intravenous contrast agents can be obtained [1, 2, 12, 13].

Magnetic resonance angiography and perfusion study

Lung MR angiography can be obtained either with or without intravenous contrast agent. Non-contrast MR angiography acquisitions have the main advantage of —avoiding exposure to gadolinium-containing contrast material. Non-contrast MR angiography can be obtained with bright- or black-blood techniques according to the suspected pathology, where the former is used to assess congenital vascular abnormalities and the latter, vascular wall involvement (such as in vasculitis) [14]. Contrast-enhanced MR angiography is still considered the most robust technique to assess pulmonary vasculature because of its higher SNR and contrast-to-noise ratio and its shorter measurements with high temporal and spatial resolution [6]. In children, contrast-enhanced MR angiography is usually used to study congenital vascular anomalies such as transposition of the great vessels, tetralogy of Fallot, anomalous pulmonary venous return and pulmonary sequestration.

Pulmonary perfusion can be performed using non-contrast or contrast-enhanced techniques. Non-contrast-enhanced techniques include arterial spin labeling (ASL) and Fourier decomposition. These techniques have been used to assess lung perfusion in children with cystic fibrosis or asthma [15, 16].

Dynamic imaging

Cine MRI studies are used to assess central airways in true dynamic conditions. Both 2-D and 3-D cine MRI can be performed. A limitation of 2-D techniques is that the trachea moves in all directions during the respiratory cycle, so a single slice could miss relevant airways pathology during trachea movement [17–19]. Cine MRI has been used to assess tracheobronchomalacia in pediatric patients, showing similar results to bronchoscopy and CT [19]. More recently, cine MRI has been used to assess vocal cord impairment in children after surgical correction of congenital laryngeal stenosis.

Cine MRI can also be used to assess diaphragmatic function in children with congenital diaphragmatic hernia [20, 21]. Further, cine MRI can visualize discontinuity of the diaphragm and can potentially help in distinguishing it from eventration. Moreover, MRI can accurately characterize hernia contents, defect location and size.

Techniques for assessing lung ventilation

Lung ventilation can be assessed with hyperpolarized gas MRI and oxygen-enhanced MRI. Alternatively, lung ventilation can also be assessed without gaseous contrast using Fourier decomposition [22]. Although hyperpolarized gas MRI can provide higher image quality and resolution than Fourier decomposition, the high cost of the gases and the need of dedicated hardware have limited its clinical implementation. Hyperpolarized gas MRI has been used in several pediatric lung diseases, including asthma, cystic fibrosis (CF), congenital diaphragmatic hernia and bronchopulmonary dysplasia. Also, oxygen-enhanced MRI has been used to assess lung ventilation in children, but poorer SNR and the long

acquisition time of this technique have hampered its broader use in the clinic [13, 16, 18].

Conversely, the free-breathing Fourier decomposition imaging is a low-cost and simple technique that provides both ventilation and perfusion images in a single acquisition. Fourier decomposition is is based on a 2-D gradient echo non-contrast-enhanced chest MRI technique that supplies perfusion and ventilation maps not dependent on intravenous or gaseous contrast agents. Fourier decomposition acquires images with high temporal resolution (3–4 images per second) in the coronal plane without cardiac or respiratory gating. Then MRI data are registered with different algorithms to compensate for respiratory motion [13, 23]. Finally, signal intensity changes of the lung parenchyma related to the cardiac and respiratory cycle are decomposed using a Fourier transform to obtain the perfusion- and ventilation-weighted images. Fourier decomposition imaging has been tested in children with CF and obtained similar diagnostic information to hyperpolarized gas MRI and contrast-enhanced MRI [24–26].

Another robust technique to assess lung ventilation abnormalities is first-pass contrast-enhanced perfusion (4-D perfusion study) [15]. It exploits the effect of hypoxic vasoconstriction and its use has been studied in cystic fibrosis.

Advances in lung magnetic resonance imaging

The central challenge of pulmonary MRI comes from the low proton density of lungs and a very rapid transverse (R2*) relaxation rate, leading to fast signal decay. However, a variety of MRI techniques to overcome these issues have been developed for imaging of the lungs. Approaches to address these challenges include ultra-short echo-time imaging (UTE), zero echo-time imaging (ZTE), dynamic imaging and the use of hyperpolarized gases.

Traditional MR pulse sequences entail excitation of a slice or volume of the body, which requires gradient rephasing of the slice after the excitation, as well as phase encoding. Both of these steps must occur prior to signal readout, which leads to severe signal loss in images from the short T2* of lung. Ultra-short echo-time imaging addresses this problem by both the redesign of excitation pulses and the use of non-Cartesian readouts so that no phase-encoding step is required [26]. The most common of these methods uses radial k-space encoding, which has the advantage of short readouts to ensure minimal T2*-related decay of signal.

However, 3-D radial imaging comes at the cost of slower scanning, and more recently sequences have used more complicated trajectories that are spiral interleaves on a conical surface, yielding faster scan times [27, 28]. An example is shown in Fig. 1. An alternative to these 3-D methods, which have long scan times, is 2-D radial imaging [29]. Most recently, we have seen several directions of active research. One is the greater enhancement of scanning efficiency. An example of this is the use of a 3-D spiral trajectory with a dynamically changing rate of spiral radius for even higher sampling efficiency than cones [30]. Another example is the use of artificial intelligence to deblur images obtained with longer readouts. A further direction of ongoing active research in this field is motion correction, including self-navigation and image-based navigators.

Zero echo time is an approach similar to UTE, but encoding gradients are ramped even before any excitation, which enables an instantaneous echo time [31, 32]. Indeed, the image quality can be superior to UTE [31, 32]. An interesting recent direction of active research entails respiratory gating of this sequence to yield 4-D images for assessing regional ventilation [33]. One of the remaining challenges with ZTE techniques is the relatively long scan times.

Beyond anatomical imaging methods, hyperpolarized MR and dynamic MR both probe lung function. For example, the use of xenon has been explored in the context of CF [34] and helium was assessed in asthma [35].

Dynamic MRI, as described, entails either obtaining multiple frames in rapid succession or gated images. In either case, the images can be assessed qualitatively, or pulmonary signal and volume can be quantitatively determined, again yielding ventilation [17, 36].

Rapid lung magnetic resonance imaging protocol

Longer acquisition times have been one of the limiting factors of lung MRI. To overcome this, Sodhi et al. [37] proposed a rapid 2-min (magnet time) MR protocol. This optimized limited protocol comprises four basic MR sequences: half-Fourier-acquisition single-shot turbo spin-echo, a PROPELLER, a true fast imaging with SSFP, and a VIBE (volumetric interpolated breath-hold examination) sequence. These four non-respiratory and non-ECG-gated MRI sequences were successfully performed in 75 children who were older than 5 years [37]. Total MRI scanning time was nearly 2 min for all four sequences, although the total magnet room time reported was 14–20 min [37]. More similar studies in future should widen the horizon for applications of lung MRI in children.

Common indications

Acute infection

The examination of pneumonia in children was one of the first indications of lung MRI to be investigated. Early experience

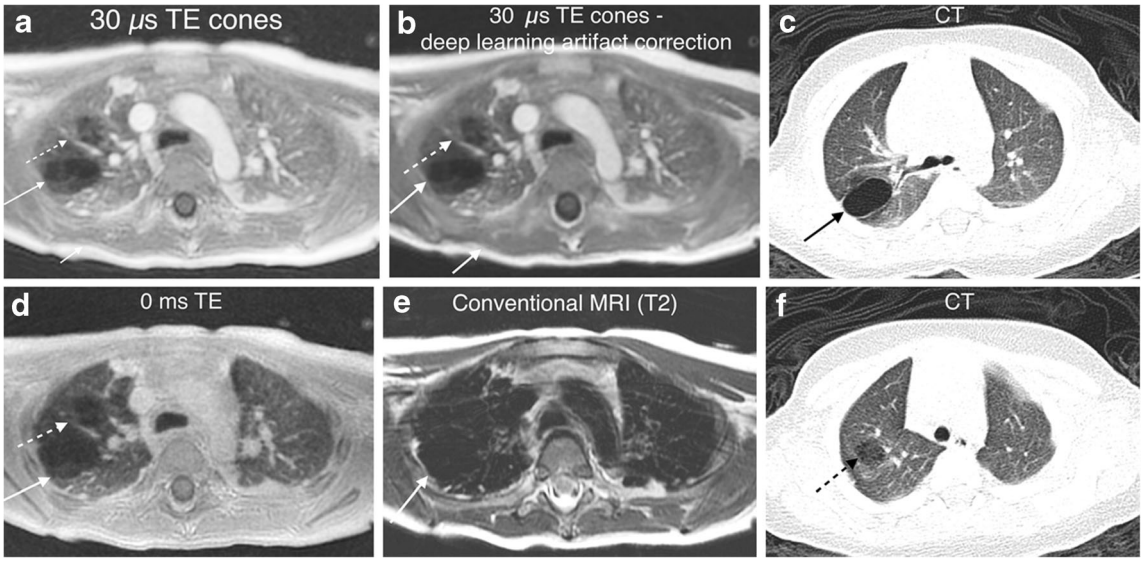

Fig. 1 Ultrafast echo-time (UTE) MRI in an 8-month-old boy with congenital pulmonary airway malformation (CPAM). **a, b** UTE images obtained with a cones readout permits a 30 μs (microsecond) echo time, with artifact (**a**) and with a neural-net-based correction to remove artifact (**b**). Notice the larger lesion (*long solid arrow*), adjacent smaller lesion (*dashed arrow*), as well as artifact from long echo time along the subcutaneous fat (*short solid arrow*). **c** Corresponding axial CT of the larger lesion. **d** An alternative is zero echo time (ZTE) imaging, which yields sharper images and higher pulmonary signal, but at the cost of increased scan time. *Solid arrow* indicates larger lesion; *dashed arrow* indicates smaller lesion. **e** Axial T2-weighted MRI. *Arrow* indicates larger lesion. **f** Corresponding axial CT of the smaller lesion. Note that the UTE (**a** and **b**) and ZTE (**d**) images have good correlation with CT delineations of the larger lesion (*arrow* in **c**) and smaller lesion (*arrow* in **f**), but the T2-weighted image (**e**) fails to capture pulmonary signal

was obtained on low-field MRI (mainly 0.2-T scanners) using SSFP sequences [38, 39]. The open design of the scanners was considered favorable for pediatric imaging. By using thick slices, short breath-hold times of 4–5 s could be achieved. While many low-field open scanners have been replaced by 1.5-T or 3-T systems, the utility of SSFP sequences is still appreciated. Community-acquired pneumonia and complications like pleural empyema can be readily examined [40, 41]. T2-W sequence as well as the SSFP sequences have an excellent sensitivity for the high contrast provided by the liquid accumulation inside pneumonic infiltrates against the black background of healthy lung tissue [9]. First reports, though in adults, suggest that even acute viral penumonia, i.e. related to severe acute respiratory syndrome coronavirus (SARS-CoV-2) disease 2019 (COVID-19), can be reliably detected with MRI [42].

While chest radiograph and lung US often serve for first-line bedside detection of acute pneumonia, lung MRI can be used in the second line as a problem-solving method for complicated findings, e.g., pulmonary abscess inside an infiltration, or central lesions that are difficult to reach with US [43] (Figs. 2 and 3).

Lung MRI has been shown to be particularly useful for detecting pulmonary infiltrates in immunocompromised children with hematologic malignancies. Currently, high-resolution CT (HRCT) is the method of choice, while radiography is considered not sensitive enough in this high-risk group. To replace HRCT with MRI to reduce radiation exposure, Sodhi et al. [44] compared both methods in 26 children with leukemia (age range 5–13 years) who presented with fever and neutropenia. Using a standard protocol based on fast spin-echo sequences (T2-W single-shot half-Fourier and rotating phase encoding), T1/T2 SSFP and T1-weighted 3-D gradient echo sequences, MRI was diagnostic for the key features (13/13 cases presenting with nodules, 8/8 presenting with consolidations and 4/6 presenting with ground-glass opacities). From this, the authors concluded that MRI would be suitable as the first-line modality to exclude pneumonia in children with leukemia and persistent febrile neutropenia [44].

Similar to children with iatrogenic immunocompromise, MRI can be recommended in cases of acquired immunodeficiency from human immunodeficiency virus (HIV) infection and suspected complicating respiratory infection. Using a 3-T scanner, Rana et al. [45] applied a similar combined protocol approach in 25 HIV-positive children with respiratory symptoms and confirmed a very high sensitivity and specificity of MRI (100%, 100%) for nodules >4 mm, pleural effusion and lymphadenopathy. Sensitivity was close to 90% for pulmonary consolidation/dystelectasis and 75% for bronchiectasis and ground-glass opacities, with specificities ranging 75–100% [45].

Chronic infection

Chronic pulmonary infections in pediatric patients comprise fungal (i.e. in immunocompromised children) or mycobacterial infections. Common pulmonary fungal infections in the pediatric population are aspergillosis, coccidioidomycosis and

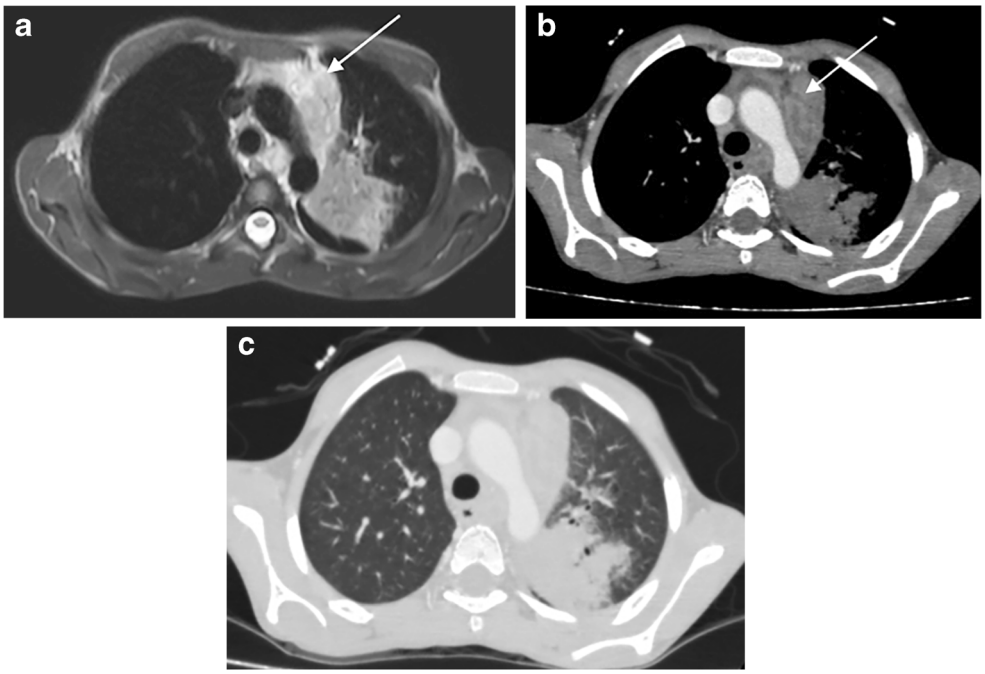

Fig. 2 Cross-sectional imaging in a 7-year-boy with acute leukemia with pneumonia on imaging. **a** Axial T2-W turbo spin-echo (TSE) MR image shows consolidation in the left upper lobe. **b, c** Axial contrast-enhanced CT images in mediastinal (**b**) and lung (**c**) windows show similar findings. There is associated mediastinal lymphadenopathy (*arrow*), which is very well appreciated on T2-W TSE (**a**) and contrast-enhanced CT mediastinal (**b**) window images

histoplasmosis. Frequently, the type of pulmonary infection is suggested by presence of different types of nodules (Fig. 4) and in many cases, by the tree-in-bud pattern with centrilobular nodules of airborne infection or a miliary pattern with hematogenic spread, respectively [3]. Key diagnostic features such as nodular lesions and consolidations can be readily detected; however, for detecting subtle changes of airway structure, MRI does not reach the sensitivity of HRCT (see "Airway disease" section on allergic bronchopulmonary aspergillosis).

For the examination of pulmonary tuberculosis, Zeng et al. [46] compared the utility of MRI and CT using a T2-W fast spin-echo sequence with rotating phase-encoding for motion compensation. In a series of 63 patients, the authors clearly identified diagnostically relevant pathology such as tree-in-bud sign, ground-glass opacity, consolidation, masses and

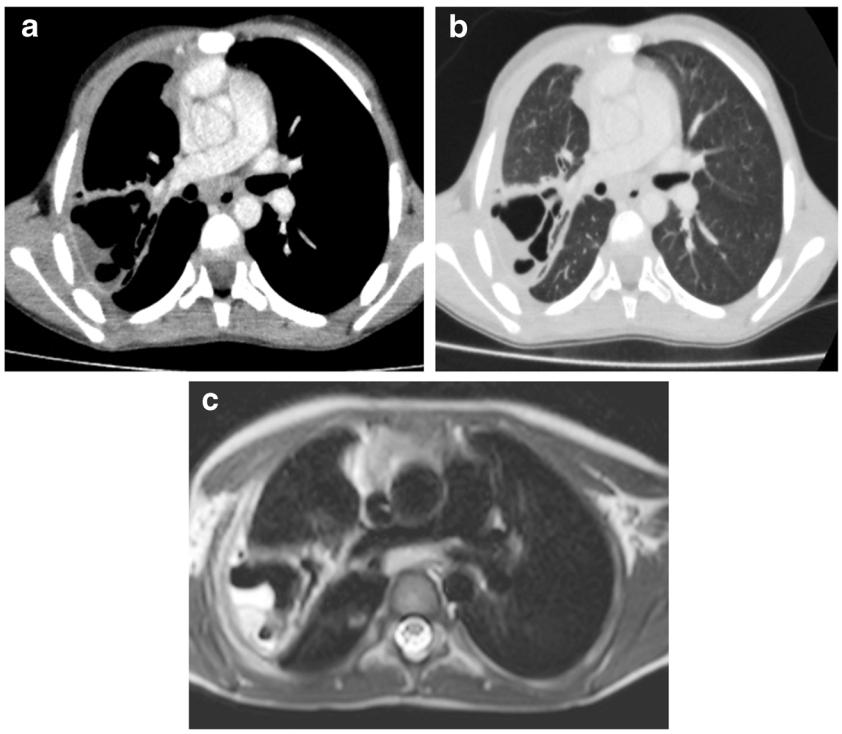

Fig. 3 Cross-sectional imaging in an 8-year-boy with lung abscess. **a, b** Axial contrast-enhanced CT images in mediastinal (**a**) and lung (**b**) windows show an area of consolidation in the right lung with cavitation and air and fluid within. **c** Axial T2-W turbo spin-echo MR image shows similar findings

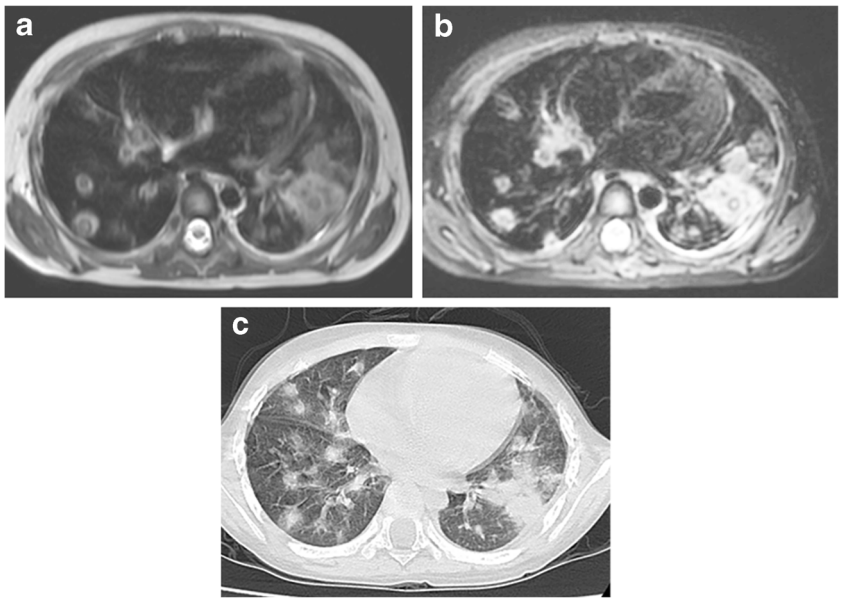

Fig. 4 Disseminated fungal infection in a 9-year-boy with febrile neutropenia. **a, b** Axial T2-W turbo spin-echo (**a**) and MultiVane XD (**b**) 3-T MR images show nodules in the bilateral lungs with target appearance and ground-glass opacities in places. **c** Corresponding high-resolution CT lung window image shows similar bilateral lung nodules with ground-glass opacities

cavitations [46]. The sensitivity for non-calcified nodular lesions was consistent with previous reports (50.0%, 91.1% and 100% for nodules sizes <5 mm, 5–10 mm and >10 mm, respectively). Completely calcified lesions or calcifications inside lesions were difficult to detect or to differentiate from other signal voids, respectively. Advantages compared to CT were observed in the detection of pleural thickening or subtle pleural effusion and in respect to soft-tissue contrast to identify caseation and liquefactive necrosis inside solid lesions [46]. Notably, these observations were made in an adult population, but they are consistent with the results of MRI in a study on 40 children, conducted with a standard lung MRI protocol based on fast spin-echo sequences (T2-W single-shot half-Fourier and rotating phase encoding), T1/T2 SSFP and T1-weighted 3-D gradient echo sequences [47]. According to the different spectrum of disease manifestations in children, the study revealed mediastinal and hilar lymphadenopathy, pleural effusion and lung cavitation (considered typical for tuberculosis) with a sensitivity and specificity of 100%. Sensitivity and specificity for nodules were 88.2% and 95.7%, respectively [47]. Kappa agreement between CT and MRI in detection of each finding was almost perfect (k=0.8–1.0) [47]. Altogether, lung MRI can be considered a veritable alternative to CT in pediatric patients with tuberculosis. Only calcifications as an important diagnostic feature might be missed; hence, for clinical application an additional chest radiograph at the baseline might be considered (Fig. 5). Lung MRI can also be used in children with chronic respiratory symptoms or middle lobe syndrome (Fig. 6).

Airway disease

Among pediatric lung diseases, airway disease associated with CF is the most thoroughly investigated, frequently examined, and by far the most standardized indication for MRI of the lung in children [48]. In children with CF, pulmonary involvement remains the most important determinant of morbidity and mortality. Under the assumption that pulmonary function testing is not sensitive enough for subclinical disease progression, imaging plays an important role in clinical monitoring

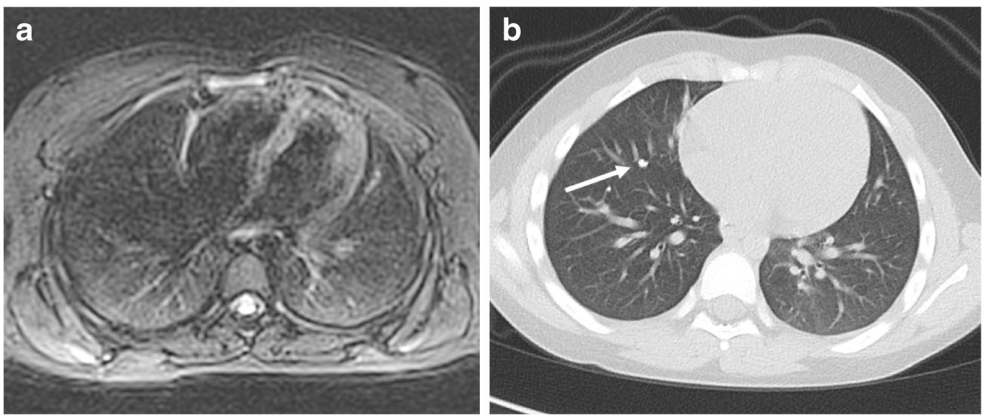

Fig. 5 Missing signal of pulmonary calcification on MRI. **a, b** Transverse T2-W MRI with fat signal suppression (**a**) and corresponding CT scan (**b**) of a 6-mm calcified pulmonary nodule (*arrow* in **b**) in a 9-year-old boy detected during examinations after pulmonary tuberculosis. Because of the complete calcification, the nodule remains invisible on the MR scan

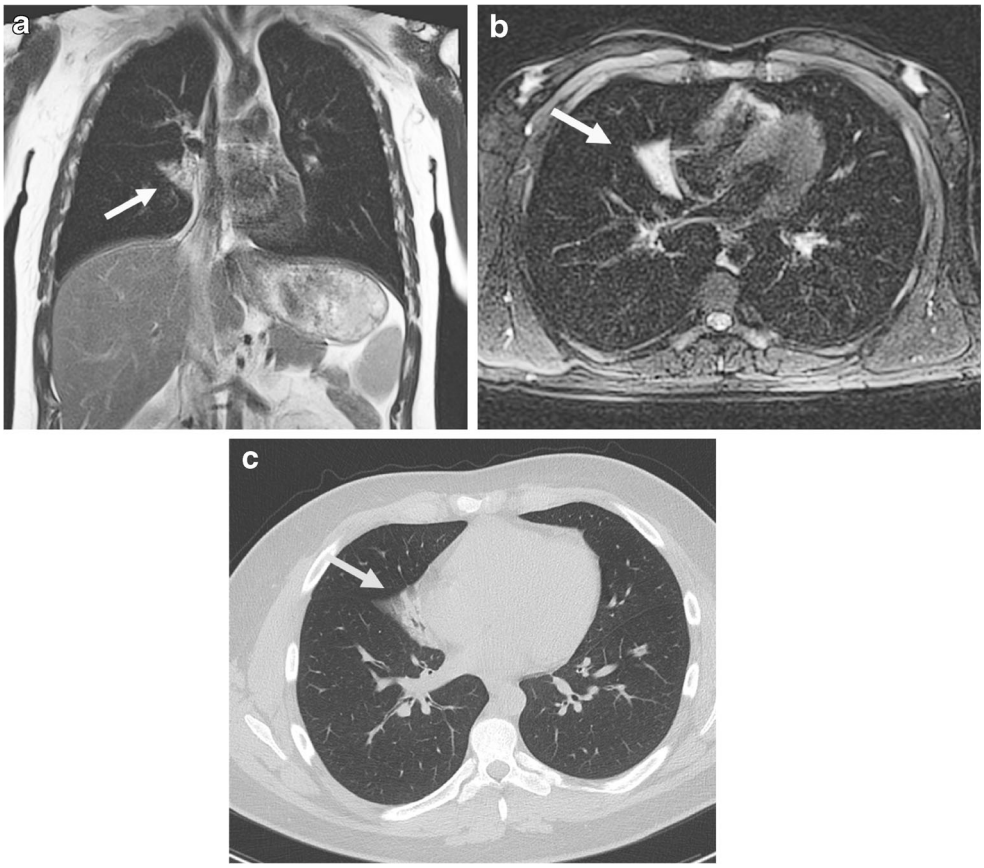

Fig. 6 Middle lobe syndrome in a 17-year-old boy with chronic recurrent respiratory symptoms. **a, b** T2-W MRI with a coronal half-Fourier fast spin-echo (**a**) and transverse fast spin-echo with fat suppression (**b**) images show a triangular consolidation with bright signal and signal voids from ectatic bronchi (*arrows*). **c** Corresponding CT plane for comparison shows similar findings (*arrow*)

and research of CF lung disease. More than any other imaging modality, MRI offers structural and functional imaging without radiation exposure [49, 50] (Fig. 7).

Current clinical practice is grounded on a general MRI protocol for state-of-the-art clinical 1.5-T scanners based on the available sequence technology [9], an adapted semiquantitative scoring system that allows for comparison with established scores for radiograph and CT [48] and validation of the concept in a multicenter setting [48]. Recommended protocols are based on chest radiograph and contrast-enhanced MRI of the lungs for initial diagnosis that can then be repeated at yearly intervals [51]. If the initial imaging is performed before 1 year of age, the first MRI is performed without contrast enhancement. CT is reserved for emergencies (e.g., pulmonary hemorrhage) or inconclusive cases [51]. The morphological sequences of the protocol were shown to be efficient in imaging bronchial wall thickening, bronchiectasis, mucus plugging, air-fluid levels, consolidation/infiltration, mosaic pattern and lobar or segmental destruction, with reasonable quality compared to CT [14, 48, 49, 51, 52]. While the diagnostic scope of MRI regarding structural information just reaches CT because of slightly lower spatial resolution and motion artifacts (resulting from longer acquisition times), its main advantage over CT is the availability of additional functional information, e.g., from perfusion imaging and real-time imaging of respiratory motion [22]. Perfusion imaging is mainly used to detect and follow perfusion deficits related to slowed or missing pulmonary ventilation in areas of bronchial obstruction (hypoxic vasoconstriction). Significant improvements of perfusion deficits after physiotherapy and antibiotic medication could be demonstrated with MRI [48]. The implemented semi-quantitative scoring system is designed to cover both morphological and functional changes based on a simple lobe analysis for the absence (scored 0), involvement by less than 50% (scored 1) and more than 50% (scored 2) of a lung lobe by six pathologies or clusters of findings (bronchiectasis/bronchial wall thickening, mucus plugging, abscesses/sacculations, consolidations, special findings and perfusion defects). When counting the lingula as a separate "left middle lobe," a maximum global score of 72 can be reached [52].

The use of gadolinium-based contrast material remains a concern, so alternative approaches based on dynamic proton MRI with Fourier decomposition of cyclic signal changes of lung parenchyma in ventilated and perfused regions [15], T1-mapping [19], oxygen-enhanced MR [22] and hyperpolarized ^{3}He [24] and ^{129}Xe [24] MRI are under investigation. However, because of the lack of robustness, the need for expensive hardware or limited availability of the necessary gases, none of these approaches has been adopted for clinical imaging routine.

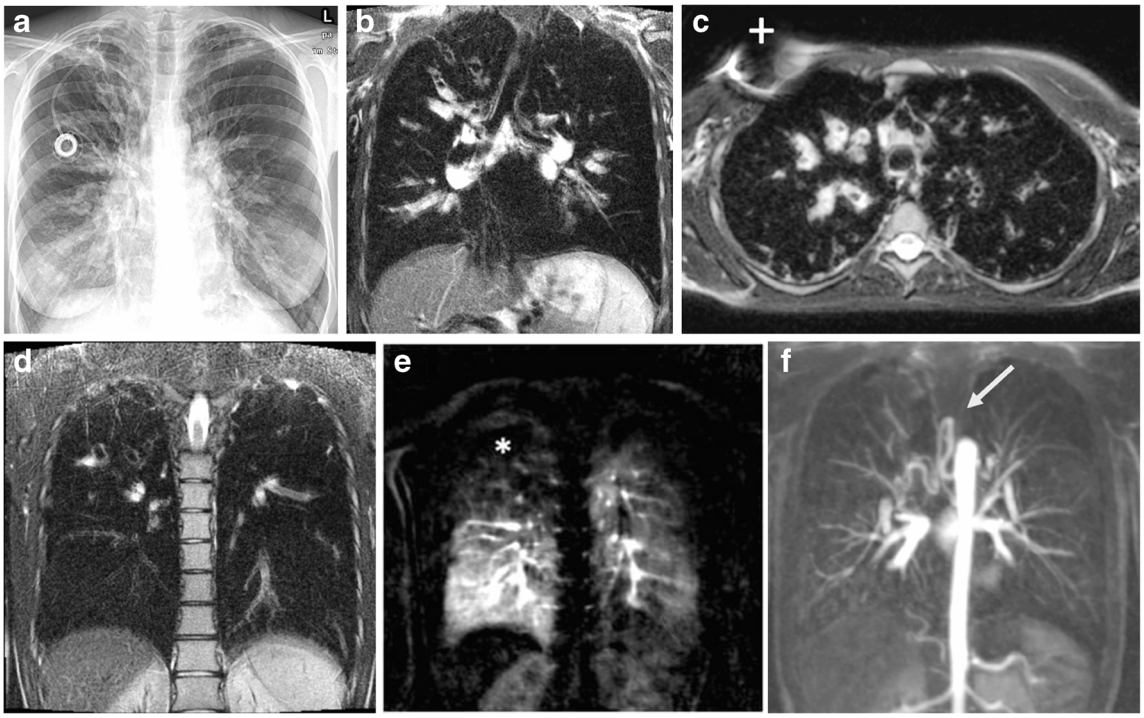

Fig. 7 Morpho-functional MRI of severe cystic fibrosis in a 15-year-old boy. **a** Posteroanterior chest radiograph. **b–d** T2-W MRI in coronal orientation at the level of the trachea (**b**), axial orientation above the aortic arch (**c**) and coronal orientation at the level of the spine (**d**) show bronchiectasis, bronchial wall thickening and mucus retention. **e** The first-pass perfusion scan demonstrates severe perfusion deficits of the upper right lung lobe from hypoxic vasoconstriction (*asterisk*). **f** Coronal maximum-intensity projection of the systemic arterial perfusion phase reveals a dilated bronchial artery as a typical finding in chronic inflammation of the bronchial system (*arrow*). An artifact results from the port catheter (*cross* in **c**). Images courtesy of M. Wielpuetz, Heidelberg, DE

Analogous to imaging children with CF, the same protocol can be readily used for imaging other diseases involving the bronchial system or related to muco-cilial dysfunction such as allergic bronchopulmonary aspergillosis (ABPA) or Kartagener syndrome (Fig. 8). In ABPA, the role of imaging is to investigate lung damage, i.e. to detect bronchiectasis (a complication that triggers the switch from inhaled corticosteroids to oral medication), while the diagnosis itself is based on immunological parameters [53, 54]. Sodhi et al. [8] included 27 people with a confirmed diagnosis of ABPA and performed lung MRI in addition to the clinically indicated HRCT scans. Imaging was performed on a 3-T scanner using fast spin-echo sequences (T2-W single-shot half-Fourier and rotating phase encoding), T1/T2-W SSFP and Dixon T1-weighted 3-D gradient echo sequences.

The sensitivity for key diagnostic features (bronchiectasis, consolidation, nodules, mucus retention) ranged 68–100%, with negative predictive values of 71–100%, the lowest for bronchiectasis and highest for mucus retention. Specificity and positive predictive values were excellent (100%) [8].

These results give good insight into the role that lung MRI can play in clinical routine airway imaging beyond cystic fibrosis as the current state of the art: a spatial resolution still slightly below that of HRCT and the susceptibility to motion artifacts not yet allowing promotion of non-contrast-enhanced MRI as a screening test for subtle changes of airway structure. If the detection of such would be crucial for therapeutic decisions, we would still recommend HRCT for the baseline examination (and switch to follow-up using MRI as far as appropriate) unless the clinical value of non-contrast-enhanced MRI has been more precisely defined. For the particular case of ABPA, no data are available from dynamic perfusion studies, but it might be assumed that analogous to cystic fibrosis, perfusion deficits resulting from hypoxic vasoconstriction could be a highly sensitive indicator for ABPA-related airway disease.

Cine MRI can also be used to assess central airways in true dynamic conditions. Both 2-D and 3-D cine MRI can be performed. Cine MRI has been used to assess tracheobronchomalacia in pediatric patients, showing similar results to bronchoscopy and CT [6, 18, 55, 56]. A recent study has described another possibility of a free-breathing fast T2-W MultiVane MRI sequence (Philips Healthcare, Best, The Netherlands), which is reported as a technically feasible and promising new MRI technique for evaluating pediatric large airways [57].

Interstitial lung disease

Imaging interstitial lung diseases remains one of the big challenges for MRI. The diagnosis and differential diagnosis of

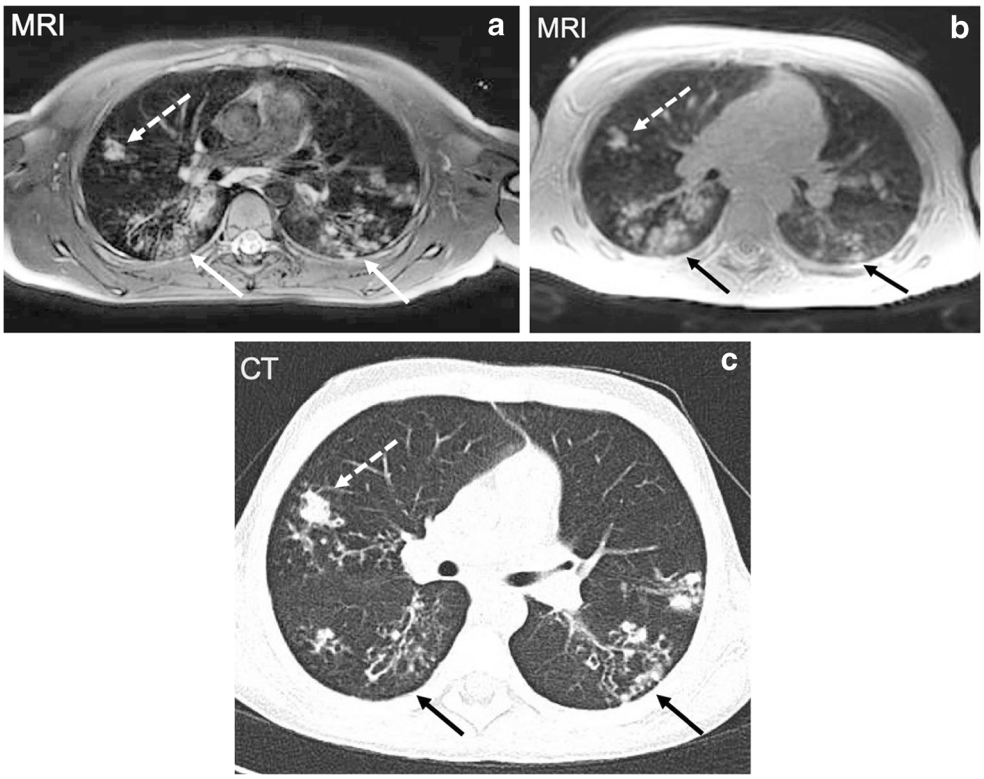

Fig. 8 Cross-sectional imaging in an 11-year-old boy with cystic fibrosis and allergic bronchopulmonary aspergillosis. **a–c** Axial T2-W turbo spin-echo PROPELLER (periodically rotated overlapping parallel lines with enhanced reconstruction), 1×1×5-mm (**a**); axial reformat 3-D ultra-short echo-time 1.5-mm isotropic image (**b**) on a 1.5-T system; and axial CT image (**c**). Note multiple areas of centrilobular nodules and mucus plugging in the lower lobes (*arrows*) and nodule in the right upper lobe (*dashed arrow*)

interstitial lung diseases are based on the detection of lesion patterns that allow for the attribution of findings to anatomical compartments of the lung, i.e. the secondary pulmonary lobule. Here, anything that was learned from CT can be readily applied in MRI. Diffuse, centrilobular or peri-lobular localizations of pathology indicate a hematogenic, bronchial or lymphatic spread of disease, respectively. In this respect, the higher spatial resolution of HRCT is considered advantageous over MRI for detecting small details and patterns (e.g., fine reticulation, ground-glass opacities and micronodules). While interlobular septal thickening can be well recognized, intralobular interstitial reticulation might not be distinguished from alveolar accumulation of fluid because both would appear as ground-glass signal on MRI because of the lower spatial resolution. However, larger details (e.g., coarse fibrosis and honeycombing) can be clearly visualized with MRI, and the capability of MRI to add clinically valuable information on regional lung function (e.g., assessment of ventilation, perfusion and mechanical properties) or inflammation to some extent compensates for deficits in spatial resolution [58] (Figs. 9 and 10). MRI is therefore already being used in adults for comprehensive cardiopulmonary imaging in sarcoidosis or for follow-up of lung fibrosis after initial correlation with CT [59]. In particular for sarcoidosis, the identification of the so-called "dark lymph node sign" in the mediastinum has been attributed a high positive predictive value for the noninvasive confirmation of sarcoidosis [60].

Acute interstitial lung diseases with interstitial infiltration and edema can be expected to present with intense signal on T2-W images; this signal decreases when cellular, interstitial

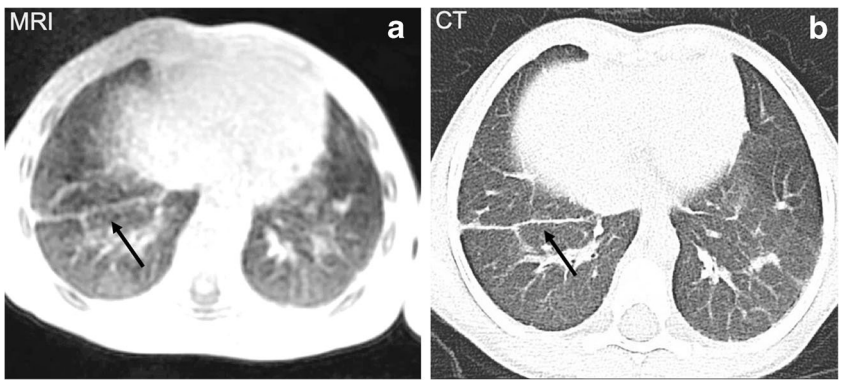

Fig. 9 Nonspecific interstitial pneumonia (pathology diagnosis) in a 5-year-old girl. **a, b** A 1.4-mm isotropic ultra-short echo-time axial reformat MRI (**a**) and 3-mm axial CT (**b**) show intralobular septal thickening (*arrow*) from interstitial pathology

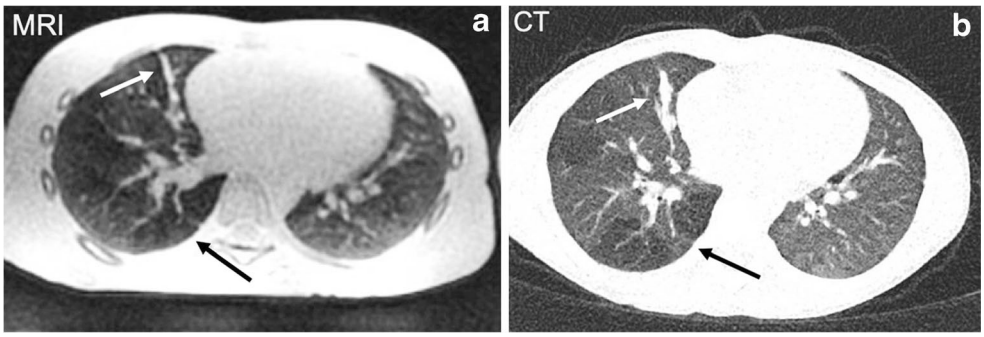

Fig. 10 Bronchopulmonary dysplasia in a 9-year-old girl. **a, b** A 1.5-mm isotropic zero echo time axial reformat free-breathing MRI (**a**) and 3-mm axial CT (**b**) show fibrotic strand on the right (*white arrow*) and hypodense/hypointense lung regions representing emphysema/air-trapping (*black arrow*)

and capillary fluid accumulation are replaced by fibrotic scarring [58]. Furthermore, pure accumulations of fluid appear as bright signal on T2-W imaging but only very low signal on T1-weighted imaging, which helps to differentiate fibrotic lesions from pulmonary congestion caused by heart failure [61]. Beyond the scope of HRCT, MRI offers functional information on lung perfusion that contributes to the estimation of lung function impairment [58]. While different approaches for the early detection of fibrosing lung disease are under investigation (e.g., contrast uptake in active fibrosis [62], T1-mapping [63] and elastic deformation analyses [64]), these have not arrived in clinical routine or not been validated in the pediatric population.

Pulmonary masses

Primary pulmonary neoplasms are an unusual finding in pediatric patients; therefore, they are often not considered in the differential diagnosis for symptomatic children with persistent pneumonitis, coughing and atelectasis [65]. The conventional chest radiograph fails in about 10% of patients to demonstrate any signs of obstruction and to show the tumor itself, and it frequently reveals only non-specific findings that might be interpreted as inflammatory unless demonstrated to be unusually persistent [66]. Clinicians might still be reluctant to use CT because of the radiation exposure, so delays in treatment are the unfortunate reality. Although large clinical studies in

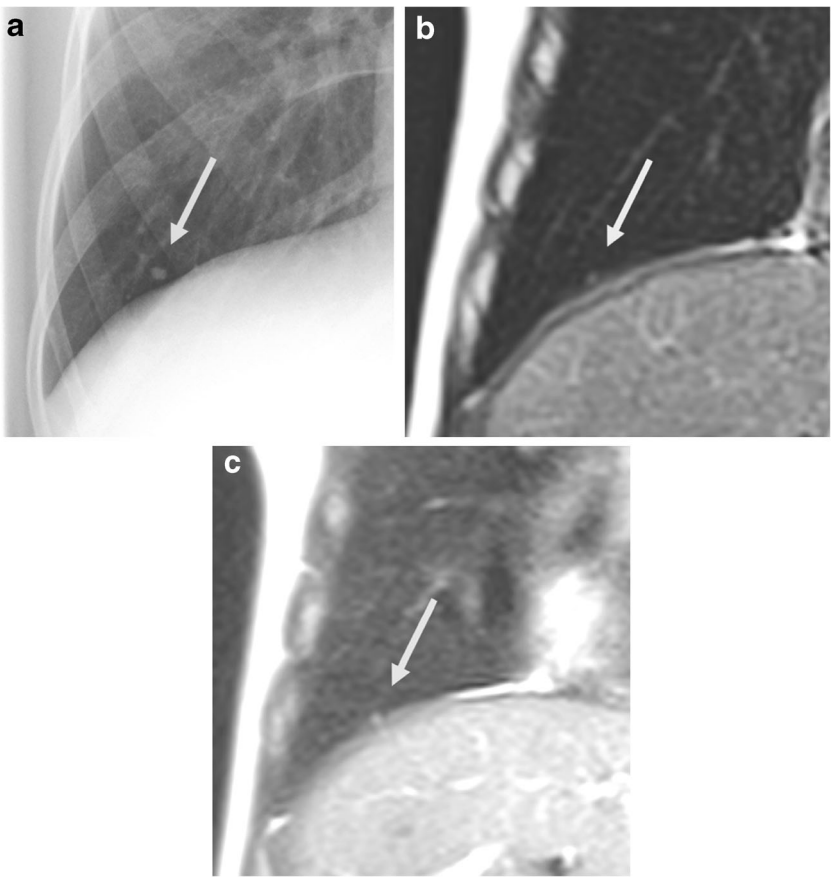

Fig. 11 Limits of MR signal and spatial resolution. A 3-mm calcified pulmonary nodule (*arrows*) was detected in a 9-year-old boy during examinations after pulmonary tuberculosis. **a–c** The amount of calcification is sufficient to render the nodule as very dense radiopacity on the posteroanterior chest radiograph (**a**), but the remaining soft-tissue component still provides enough signal to allow for nodule detection on coronal T2-W fast spin-echo (**b**) and half-Fourier fast spin-echo (**c**) MR images

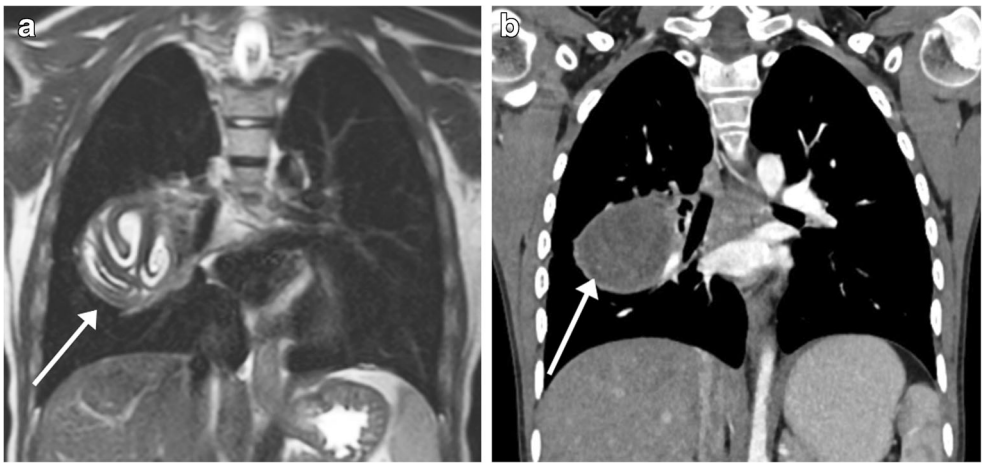

Fig. 12 Hydatid cyst in a 10-year-boy. **a** Coronal T2-W turbo spin-echo 3-T MR image shows a well-defined cystic lesion (*arrow*) in the right lung with curvilinear internal membranes. **b** The membranes are not well appreciated within the mass (*arrow*) on corresponding coronal contrast-enhanced CT mediastinal window image. These internal membranes are a characteristic feature of hydatid cyst

this context have not been performed because of the rareness of cases, it is believed that MRI offers all necessary properties not only to detect malignant lesions, but also to further differentiate them from simple consolidation of pneumonic infiltration, relying on its superior soft-tissue contrast [67]. Instead of hesitating to use CT, it might, therefore, be recommended to apply MRI in cases of unconclusive or suspicious findings on chest radiographs.

The majority of tumors involving the lungs in children are metastatic (i.e. Wilms tumor, osteosarcoma, Ewing sarcoma and lymphoma). Among the rare primary lung tumors, approximately 75% are malignant, e.g., pleuropulmonary blastoma, pulmonary carcinoid tumor, mucoepidermoid tumor, epithelioid hemangioendothelioma and bronchogenic carcinoma [65, 68]. The differential diagnosis comprises pulmonary hamartoma, pulmonary chondroma, respiratory papillomatosis, pulmonary sclerosing pneumocytoma, pulmonary inflammatory myofibroblastic tumor, pleural fibrous pseudotumor or parasitic lesions [68]. Notably, completely calcified lesions appear with low signal intensity, therefore MRI might not be recommended for metastases of osteosarcoma [69]. Given the only slightly inferior sensitivity for pulmonary nodules compared to CT, MRI might be recommended for long-term follow-up of children and young adults after malignancies with potential mediastinal and pulmonary metastases, e.g., in children with seminoma. For this purpose, a threshold size of 4–5 mm can be expected for pulmonary nodule detection with MRI [33, 70–72] (Fig. 11). In metastatic disease with pleural effusion, MRI might be helpful to differentiate reactive pleural effusions (simple fluid, hypointense on T1-W images and hyperintense on T2-W images) from metastatic spread to the pleura (effusion accompanied by pleural nodularity, pleural enhancement, septations of the fluid) [68].

In the differentiation of solid and cystic lesions, the high soft-tissue contrast of MRI is highly appreciated (Fig. 12). As discussed, cystic lesions appear with particularly bright signal against the dark background of healthy lung tissue. This is appreciated when applying MRI for the evaluation of pulmonary hydatid disease in children (Fig. 12). In a prospective trial including 28 children with clinically suspected pulmonary hydatid disease, Sodhi et al. [73] confirmed an equivalent diagnostic accuracy of non-contrast-enhanced MRI compared to contrast-enhanced multi-detector CT. Imaging was performed on 1.5-T and 3-T scanners using a similar protocol set-up with fast spin-echo sequences (T2-W single-shot half-Fourier and rotating phase encoding), T1/T2-W SSFP and Dixon T1-weighted 3-D gradient echo sequences. Both MRI and CT reached accuracy >90% for the detection of hydatid cysts, while MRI proved to be more sensitive than CT scan for intra-cystic membranes and provided a 28.6% rise in diagnostic value when directly compared to CT scan.

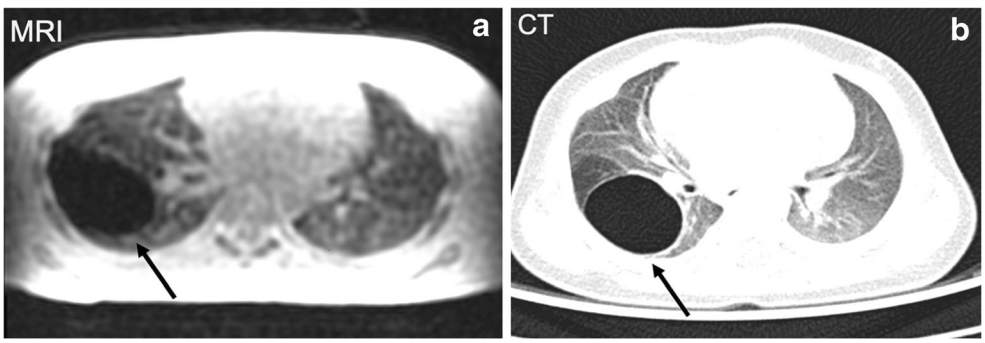

Fig. 13 Congenital pulmonary airway malformation (CPAM) type 1 in a 12-year-boy. **a, b** Axial reformat proton-density 3-D spoiled gradient recalled echo 3-mm isotropic MR image (at 1.5 T) at 12 years of age (**a**) and axial CT image obtained at 4 months of age (**b**). Note the large oval lesion with signal void in the right lower lobe (superior segment) and the corresponding gas-filled cyst on CT (*arrows*)

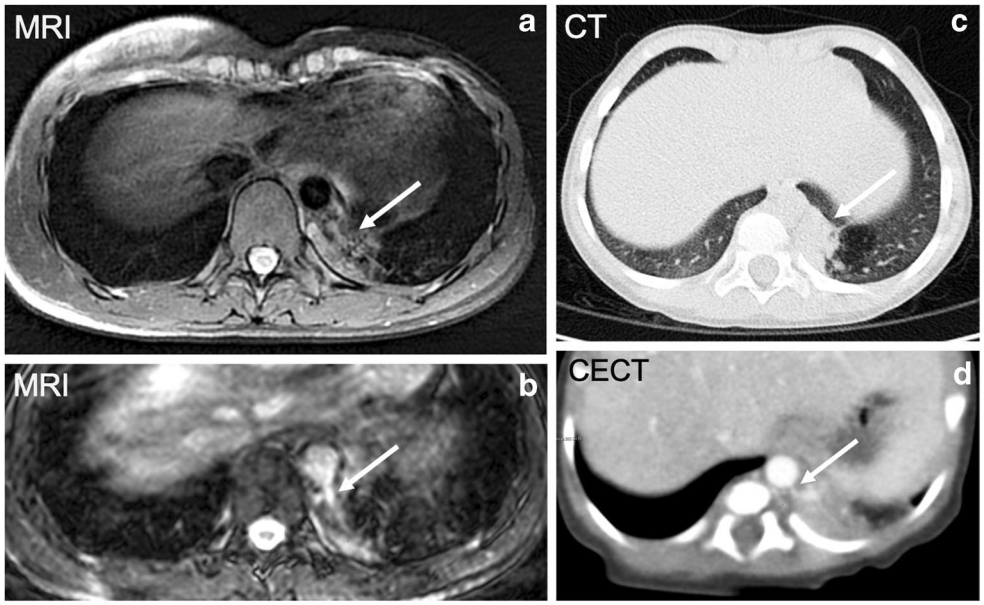

Fig. 14 Sequestration in the left lower lobe in a 15-year-old boy. **a–d** Axial T2-W turbo spin echo PROPELLER (periodically rotated overlapping parallel lines with enhanced reconstruction) (**a**), axial reformat 3-D fast imaging employing steady-state acquisition (FIESTA) (**b**) on a 1.5-T MR system, and axial CT images obtained at 3 years (**c**) and at 1 month (**d**) of age. Note soft-tissue lesion in the left lower lobe (*arrow* in **a**) with aberrant systemic artery arising from the descending aorta (*arrow* in **b**). Note in (**c**) a similar soft-tissue lesion in the same location (*arrow* in **c**) and an abnormal vessel arising from descending thoracic aorta (*arrow* in **d**)

Congenital malformations

Given the diagnostic scope of MRI for detecting various categories of findings as described here, it is not surprising that MRI is considered a useful modality for evaluating congenital malformations (Figs. 13, 14, 15 and 16). For example, Zirpoli et al. [74] investigated lung MRI for the evaluation of congenital malformations of the lung using respiration-triggered T2- and T1-weighted fast spin-echo sequences and a fast SSFP gradient echo sequence. The non-contrast-enhanced MRI protocol proved to be efficient in the detection of congenital pulmonary airway malformation, segmental bronchial atresia, bronchopulmonary sequestration, congenital lobar overinflation, bronchogenic cyst and hybrid lesions, thus allowing for a correct diagnosis in 19/20 patients (22/23 malformations) [74]. The authors observed a relative weakness compared to CT in the detection of abnormal vascularization, in particular in the lower lobe paravertebral region [74]. This could be mainly attributed to the fact that the CT scans were obtained after application of intravenous contrast material, whereas the MRI scans remained unenhanced [69, 74]. It might, therefore, be recommended to add a contrast-enhanced perfusion study and an angiogram to the protocol in select cases [3]. Cine MRI can also be used to assess diaphragmatic function in children with congenital diaphragmatic hernia. Cine MRI can

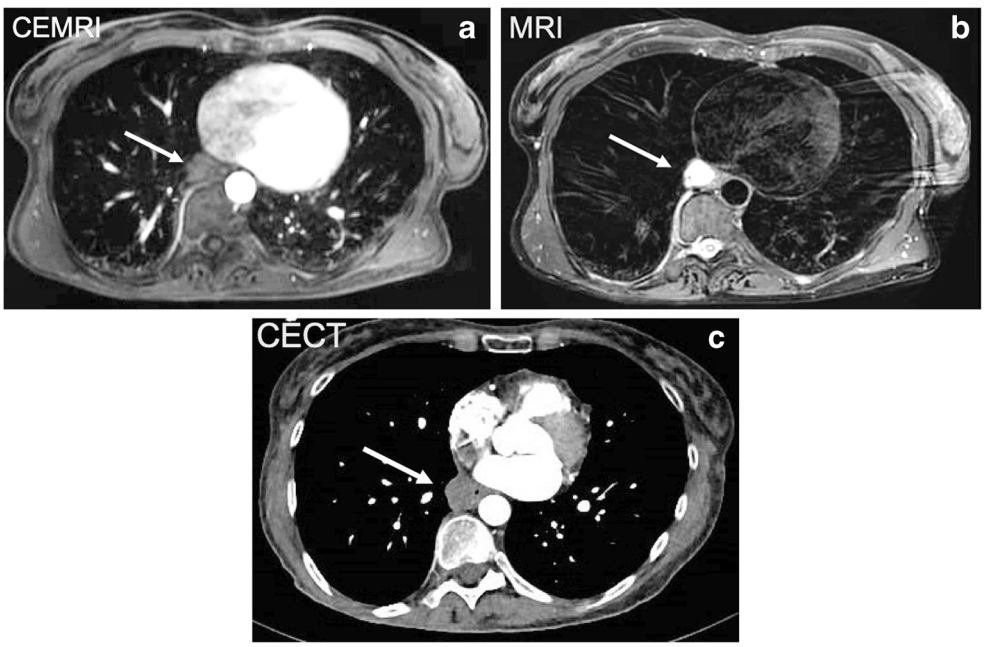

Fig. 15 Paraesophageal cystic lesion of the right posterior mediastinum (esophageal duplication cyst) in an 18-year-old woman. **a–c** T1-W post-contrast spoiled gradient recalled echo (SPGR) (**a**), T2-W axial turbo-spin echo PROPELLER (periodically rotated overlapping parallel lines with enhanced reconstruction) (**b**), and axial CT post-contrast (**c**) images. Note there is no contrast enhancement on either MRI (*arrow* in **a**) or CT (*arrow* in **c**), and the high signal intensity on T2-W imaging; these findings indicate fluid content (*arrow* in **b**)

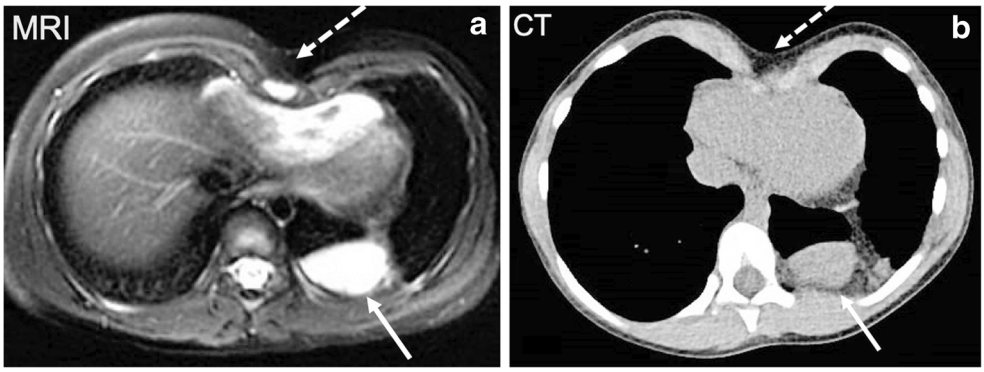

Fig. 16 Congenital diaphragmatic hernia on the left side and herniation of stomach in an 11-year-old girl. **a, b** A 2-mm isotropic T2-W turbo spin-echo axial reformat free-breathing MRI (**a**) and 3-mm axial CT soft-tissue window (**b**). Note herniation of stomach (*solid arrow*) and pectus excavatum (*dashed arrow*)

visualize discontinuity of the diaphragm and distinguish it from eventration [20, 21]. MRI can also accurately characterize hernia contents, defect location and size.

Limitations of magnetic resonance imaging

Lung MRI theoretically has several disadvantages compared to CT. The longer acquisition times in most of the MR protocols limit the use of MRI in dyspneic children who cannot lie long in the scanner. MRI is susceptible to image degradation from breathing and cardiac motion, and patient motion. In younger children, the need of anesthesia can facilitate the development of atelectasis, which might obscure underlying lung pathology. These factors make the implementation of MRI protocols difficult at centers with less expertise. Finally, availability in low-resource settings and the lack of standardization among MRI vendors determines a significant difference in image quality, even when using similar acquisition scenarios. This issue often makes it difficult to homogenize image quality across hospitals and to enable a broader use of lung MRI.

Conclusion

Lung MRI offers a radiation-free alternative to CT and can provide both anatomical and functional assessment of the chest in the same sitting. It is possible to improve image quality of lung MRI in children with proper MRI protocols and to reduce MRI scan time with judicious planning and adapting tailored MR protocols. MRI should be considered as a feasible alternative to CT scan in the evaluation of lung diseases in children. With ongoing advances in MRI technology, its applications in children are poised for wider use in the future.

Declarations

Conflicts of interest Dr. Ciet has received funds from Vertex Pharmaceutical for a study unrelated to this manuscript. Dr. Vasanawala has a research collaboration with GE Healthcare. Dr. Biederer has a scientific collaboration on MRI sequence testing and development with Siemens Healthcare.

References

1. Sodhi KS, Lee EY (2014) What all physicians should know about the potential radiation risk that computed tomography poses for paediatric patients. Acta Paediatr 103:807–811
2. Tiddens HAWM, Kuo W, van Straten M et al (2018) Paediatric lung imaging: the times they are a-changin. Eur Respir Rev 27: 170097
3. Liszewski MC, Ciet P, Lee EY (2019) MR imaging of lungs and airways in children. Magn Reson Imaging Clin N Am 27:201–225
4. Salamon ER, Lever S, Kuo W et al (2015) Spirometer guided chest imaging in children: it is worth the effort. Pediatr Pulmonol 52:48–56
5. Ciet P, Tiddens HAWM, Wielopolski PA et al (2015) Magnetic resonance imaging in children: common problems and possible solutions for lung and airways imaging. Pediatr Radiol 45:1901–1915
6. Ciet P, Wielopolski P, Manniesing R et al (2014) Spirometer-controlled cine magnetic resonance imaging used to diagnose tracheobronchomalacia in paediatric patients. Eur Respir J 43: 115–124
7. Sodhi KS, Sharma M, Lee EY et al (2018) Diagnostic utility of 3T lung MRI in children with interstitial lung disease: a prospective pilot study. Acad Radiol 25:380–386
8. Sodhi KS, Gupta P, Shrivastav A et al (2019) Evaluation of 3 T lung magnetic resonance imaging in children with allergic bronchopulmonary aspergillosis: pilot study. Eur J Radiol 111:88–92
9. Biederer J, Beer M, Hirsch W et al (2012) MRI of the lung (2/3). Why … when … how? Insights Imaging 3:355–371
10. Nguyen AH, Perez-Rovira A, Wielopolski PA et al (2018) Technical challenges of quantitative chest MRI data analysis in a large cohort pediatric study. Eur Radiol 29:2770–2782
11. Elders B, Ciet P, Tiddens H et al (2021) Magnetic resonance imaging of the upper airways in children and young adults: the MUSIC study. Thorax 76:44–52
12. Kruger SJ, Nagle SK, Couch MJ et al (2015) Functional imaging of the lungs with gas agents. J Magn Reson Imaging 43:295–315
13. Voskrebenzev A, Gutberlet M, Kaireit TF et al (2017) Low-pass imaging of dynamic acquisitions (LIDA) with a group-oriented registration (GOREG) for proton MR imaging of lung ventilation. Magn Reason Med 78:1496–1505
14. Miyazaki M, Akahane M (2012) Non-contrast enhanced MR angiography: established techniques. J Magn Reson Imaging 35:1–19
15. Wielpütz MO, Puderbach M, Kopp-Schneider A et al (2014) Magnetic resonance imaging detects changes in structure and

perfusion, and response to therapy in early cystic fibrosis lung disease. Am J Respir Crit Care Med 189:956–965
16. Zha W, Kruger SJ, Johnson KM et al (2018) Pulmonary ventilation imaging in asthma and cystic fibrosis using oxygen-enhanced 3D radial ultrashort echo time MRI. J Magn Reson Imaging 47:1287–1297
17. Tong Y, Udupa JK, McDonough JM et al (2019) Quantitative dynamic thoracic MRI: application to thoracic insufficiency syndrome in pediatric patients. Radiology 292:206–213
18. Bauman G, Puderbach M, Deimling M et al (2009) Non-contrast-enhanced perfusion and ventilation assessment of the human lung by means of Fourier decomposition in proton MRI. Magn Reson Med 62:656–664
19. Faust RA, Rimell FL, Remley KB (2002) Cine magnetic resonance imaging for evaluation of focal tracheomalacia: innominate artery compression syndrome. Int J Pediatr Otorhinolaryngol 65:27–33
20. Le Pimpec-Barthes F, Hernigou A, Mazzella A et al (2019) Dynamic magnetic resonance imaging in unilateral diaphragm eventration: knowledge improvement before and after plication. J Thorac Dis 11:3467–3475
21. Kim W, Courtier J, Morin C et al (2017) Postnatal MRI for CDH: a pictorial review of late-presenting and recurrent diaphragmatic defects. Clin Imaging 43:158–164
22. Triphan SMF, Stahl M, Jobst BJ et al (2020) Echo time-dependence of observed lung T 1 in patients with cystic fibrosis and correlation with clinical metrics. J Magn Reson Imaging 52:1645–1654
23. Bauman G, Bieri O (2017) Matrix pencil decomposition of time-resolved proton MRI for robust and improved assessment of pulmonary ventilation and perfusion. Magn Reson Med 77:336–342
24. Zha W, Nagle SK, Cadman RV et al (2019) Three-dimensional isotropic functional imaging of cystic fibrosis using oxygen-enhanced MRI: comparison with hyperpolarized ^{3}He MRI. Radiology 290:229–237
25. Rayment JH, Couch MJ, McDonald N et al (2019) Hyperpolarised (129) Xe magnetic resonance imaging to monitor treatment response in children with cystic fibrosis. Eur Respir J 53:1802188
26. Johnson KM, Fain SB, Schiebler ML, Nagle S (2013) Optimized 3D ultrashort echo time pulmonary MRI. Magn Reson Med 70:1241–1250
27. Zeimpekis KG, Geiger J, Wiesinger F et al (2020) Three-dimensional magnetic resonance imaging ultrashort echo-time cones for assessing lung density in pediatric patients. Pediatr Radiol 51:57–65
28. Zucker EJ, Cheng JY, Haldipur A et al (2018) Free-breathing pediatric chest MRI: performance of self-navigated golden-angle ordered conical ultrashort echo time acquisition. J Magn Reson Imaging 47:200–209
29. Balasch A, Metze P, Stumpf K et al (2020) 2D ultrashort echo-time functional lung imaging. J Magn Reson Imaging 52:1637–1644
30. Willmering MM, Robison RK, Wang H et al (2019) Implementation of the FLORET UTE sequence for lung imaging. Magn Reson Med 82:1091–1100
31. Bae K, Jeon KN, Hwang MJ et al (2019) Comparison of lung imaging using three-dimensional ultrashort echo time and zero echo time sequences: preliminary study. Eur Radiol 29:2253–2262
32. Madio DP, Lowe IJ (1995) Ultra-fast imaging using low flip angles and FIDs. Magn Reson Med 34:525–529
33. Bae K, Jeon KN, Hwang MJ et al (2020) Respiratory motion-resolved four-dimensional zero echo time (4D ZTE) lung MRI using retrospective soft gating: feasibility and image quality compared with 3D ZTE. Eur Radiol 30:5130–5138
34. Couch MJ, Munidasa S, Rayment JH et al (2020) Comparison of functional free-breathing pulmonary ^{1}H and hyperpolarized ^{129}Xe magnetic resonance imaging in pediatric cystic fibrosis. Acad Radiol. https://doi.org/10.1016/j.acra.2020.05.00
35. Altes TA, Powers PL, Knight-Scott J et al (2001) Hyperpolarized ^{3}He MR lung ventilation imaging in asthmatics: preliminary findings. J Magn Reson Imaging 13:378–384
36. Tong Y, Udupa JK, Wileyto EP et al (2018) Quantitative dynamic MRI (QdMRI) volumetric analysis of pediatric patients with thoracic insufficiency syndrome. Proc SPIE Int Soc Opt Eng 10578:1057806
37. Sodhi KS, Khandelwal N, Saxena AK et al (2016) Rapid lung MRI in children with pulmonary infections: time to change our diagnostic algorithms. J Magn Reson Imaging 43:1196–1206
38. Abolmaali ND, Schmitt J, Krauss S et al (2004) MR imaging of lung parenchyma at 0.2 T: evaluation of imaging techniques, comparative study with chest radiography and interobserver analysis. Eur Radiol 14:703–708
39. Rupprecht T, Böwing B, Kuth R et al (2002) Steady-state free precession projection MRI as a potential alternative to the conventional chest radiograph in pediatric patients with suspected pneumonia. Eur Radiol 12:2752–2756
40. Ley-Zaporozhan J, Ley S, Sommerburg O et al (2009) Clinical application of MRI in children for the assessment of pulmonary diseases. Rofo 181:419–432
41. Liszewski MC, Görkem S, Sodhi KS, Lee EY (2017) Lung magnetic resonance imaging for pneumonia in children. Pediatr Radiol 47:1420–1430
42. Ates OF, Taydas O, Dheir H (2020) Thorax magnetic resonance imaging findings in patients with coronavirus disease (COVID-19). Acad Radiol 27:1373–1378
43. Konietzke P, Mueller J, Wuennemann F et al (2020) The value of chest magnetic resonance imaging compared to chest radiographs with and without additional lung ultrasound in children with complicated pneumonia. PLoS One 15:e0230252
44. Sodhi KS, Khandelwal N, Saxena AK et al (2016) Rapid lung MRI — paradigm shift in evaluation of febrile neutropenia in children with leukemia: a pilot study. Leuk Lymphoma 57:70–75
45. Rana P, Sodhi KS, Bhatia A et al (2020) Diagnostic accuracy of 3-T lung magnetic resonance imaging in human immunodeficiency virus-positive children. Pediatr Radiol 50:38–45
46. Zeng J, Liu Z, Shen G et al (2019) MRI evaluation of pulmonary lesions and lung tissue changes induced by tuberculosis. Int J Infect Dis 82:138–146
47. Sodhi KS, Sharma M, Saxena AK et al (2017) MRI in thoracic tuberculosis of children. Indian J Pediatr 84:670–676
48. Wielpütz MO, von Stackelberg O, Stahl M et al (2018) Multicentre standardisation of chest MRI as radiation-free outcome measure of lung disease in young children with cystic fibrosis. J Cyst Fibros 17:518–527
49. Leutz-Schmidt P, Eichinger M, Stahl M et al (2019) Ten years of chest MRI for patients with cystic fibrosis: translation from the bench to clinical routine. Radiologe 59:10–20
50. Sodhi KS (2021) Lung MRI in children: the road less travelled. Indian J Radiol Imaging. https://doi.org/10.1055/s-0041-1729126
51. Wielpütz MO, Eichinger M, Biederer J et al (2016) Imaging of cystic fibrosis lung disease and clinical interpretation. Rofo 188:834–845
52. Eichinger M, Optazaite D-E, Kopp-Schneider A et al (2012) Morphologic and functional scoring of cystic fibrosis lung disease using MRI. Eur J Radiol 81:1321–1329
53. Sehgal IS, Agarwal R (2017) Is treatment of serological ABPA similar to that of ABPA with bronchiectasis? J Allergy Clin Immunol Pract 5:1474
54. Garg MK, Gupta P, Agarwal R et al (2015) MRI: a new paradigm in imaging evaluation of allergic bronchopulmonary aspergillosis? Chest 147:e58–e59
55. Ciet P, Boiselle PM, Heidinger B et al (2017) Cine MRI of tracheal dynamics in healthy volunteers and patients with tracheobronchomalacia. AJR Am J Roentgenol 209:757–761

56. Liszewski MC, Ciet P, Sodhi KS, Lee EY (2017) Updates on MRI evaluation of pediatric large airways. AJR Am J Roentgenol 208: 971–981
57. Sodhi KS, Bhatia A, Lee EY (2021) Prospective evaluation of free-breathing fast T2-weighted MultiVane-XD sequence at 3-T MRI for large airway assessment in pediatric patients. AJR Am J Roentgenol. https://doi.org/10.2214/AJR.20.23225
58. Biederer J, Wielpütz MO, Jobst BJ, Dinkel J (2014) MRI of interstitial lung diseases: what is possible? Radiologe 54:1204–1212
59. Chung JH, Little BP, Forssen AV et al (2013) Proton MRI in the evaluation of pulmonary sarcoidosis: comparison to chest CT. Eur J Radiol 82:2378–2385
60. Chung JH, Cox CW, Forssen AV et al (2014) The dark lymph node sign on magnetic resonance imaging: a novel finding in patients with sarcoidosis. J Thorac Imaging 29:125–129
61. Biederer J, Busse I, Grimm J et al (2002) Sensitivity of MRI in detecting alveolar infiltrates: experimental studies. Rofo 174: 1033–1039
62. Yi CA, Lee KS, Han J et al (2008) 3-T MRI for differentiating inflammation- and fibrosis-predominant lesions of usual and non-specific interstitial pneumonia: comparison study with pathologic correlation. AJR Am J Roentgenol 190:878–885
63. Mirsadraee S, Tse M, Kershaw L et al (2016) T1 characteristics of interstitial pulmonary fibrosis on 3T MRI — a predictor of early interstitial change? Quant Imaging Med Surg 6:42–49
64. Chassagnon G, Martin C, Marini R et al (2019) Use of elastic registration in pulmonary MRI for the assessment of pulmonary fibrosis in patients with systemic sclerosis. Radiology 291:487–492
65. Balassy C, Kulemann V, Hörmann M (2008) Malignant pulmonary tumors in children. Radiologe 48:955–961
66. Altman RL, Miller WE, Carr DT et al (1973) Radiographic appearance of bronchial carcinoid. Thorax 28:433–434
67. Karaman A (2020) Thoracic magnetic resonance imaging applications in children. Eurasian J Med 52:94–97
68. Liszewski MC, Ciet P, Lee EY (2020) Lung and pleura. In: Lee EY, Liszewski MC, Gee MS et al (eds) Pediatric body MRI. Springer International Publishing, Cham, pp 1–28
69. Hirsch FW, Sorge I, Vogel-Claussen J et al (2020) The current status and further prospects for lung magnetic resonance imaging in pediatric radiology. Pediatr Radiol 50:734–749
70. Meier-Schroers M, Homsi R, Skowasch D et al (2017) Lung cancer screening with MRI: results of the first screening round. J Cancer Res Clin Oncol 1444:117–125
71. Singh R, Garg M, Sodhi KS et al (2020) Diagnostic accuracy of magnetic resonance imaging in the evaluation of pulmonary infections in immunocompromised patients. Pol J Radiol 85:e53–e61
72. Sodhi KS, Bhalla AS, Mahomed N, Laya BF (2017) Imaging of thoracic tuberculosis in children: current and future directions. Pediatr Radiol 47:1260–1268
73. Sodhi KS, Bhatia A, Samujh R et al (2019) Prospective comparison of MRI and contrast-enhanced MDCT for evaluation of pediatric pulmonary hydatid disease: added diagnostic value of MRI. AJR Am J Roentgenol 212:982–987
74. Zirpoli S, Munari AM, Primolevo A et al (2019) Agreement between magnetic resonance imaging and computed tomography in the postnatal evaluation of congenital lung malformations: a pilot study. Eur Radiol 29:4544–4554